PCCP

Accepted Manuscript

ROYAL SOCIETY OF CHEMISTRY

www.rsc.org/pccp

Electrochemical Investigation of the Role of MnO_2 Nanorod Catalysts in Water Containing and Anhydrous Electrolytes for Li-O_2 Battery Applications

Hugh Geaney[a,b] and Colm O'Dwyer[a,b]*

[a] *Department of Chemistry, University College Cork, Cork, Ireland*

[b] *Micro & Nanoelectronics Centre, Tyndall National Institute, Lee Maltings, Cork, Ireland*

Abstract

The electrochemical behaviour of MnO_2 nanorod and Super P carbon based Li-O_2 battery cathodes in water-containing sulfolane and anhydrous DMSO electrolytes are shown to be linked to specific discharge product formation. During discharge, large layered spherical agglomerates of LiOH were characteristically formed on the MnO_2 cathodes while smaller, toroidal, spherical Li_2O_2 particles and films were formed on the Super P cathodes. In an anhydrous DMSO based electrolyte the LiOH structures were also found on cathodes discharged in the anhydrous electrolyte, suggesting that MnO_2 initiates electrochemical decomposition of the DMSO electrolyte to form LiOH via H_2O reactions with Li_2O_2. The LiOH crystals are uniquely formed on MnO_2, and segregated to this phase even in mixed oxide/carbon cathodes. In contrast, no Li_2O_2 toroids were noted on Super P cathodes discharged in the DMSO based electrolytes. Instead, the morphology varied from smaller sheets (at high discharge current) to much larger agglomerates (at low discharge currents). In mixed carbon/MnO_2 nanorod cathodes, the use of PVDF initiates H_2O formation that affects discharge products and an overall mechanism governing phase formation at MnO_2 in sulfolane and anhydrous DMSO with and without PVDF binder is presented. This work

highlights the importance of careful consideration of electrolyte/cathode material/discharge product interactions in the search for more stable Li-O_2 systems.

Introduction

Li-air (or Li-O_2) battery systems have recently been the subject of intense research interest as they offer the possibility of outperforming Li-ion batteries currently used in devices ranging from cell phones to electric cars.[1-8] One reason behind the exceptionally high theoretical capacity (3505 $Whkg^{-1}$) of Li-O_2 batteries is the fact that the battery chemistry differs significantly from conventional Li-ion cells.[9-11] Li-O_2 battery operation involves the reversible formation and decomposition of Li_2O_2 on a porous cathode.[12] The most promising Li-O_2 battery architecture involves a Li anode, an organic electrolyte/separator and a porous cathode. The cathode serves the dual purpose of facilitating the oxygen reduction reaction (ORR) and oxygen evolution reaction (OER) associated with discharging and charging respectively, and it also accommodates the discharge products.[13] However, several practical hurdles such as poor rate capability and limited cycle life (caused by various instabilities) must be overcome if these batteries are to become a realistic replacement for current Li-ion technologies.[14-16]

The majority of research to date has focused on cathode optimisation for Li-O_2 batteries. Initially, pure porous carbon cathodes (on a suitable porous current collector) were highlighted as they allowed for a high first discharge capacity.[13, 17, 18] However, high capacities were typically offset by poor cyclability of the carbon cathodes with rapid capacity fading noted even from the first charge. This poor cycle life for carbon cathodes is due to a combination of cathode and electrolyte instability.[19-22] Many catalyst systems have been investigated for Li-O_2 battery applications with the aim of improving cycle life and reducing overpotentials associated with charging.[23] These materials have taken the form of various nanostructured metal oxides (MnO_2,[24-29] Co_3O_4[30-32]) and noble metals and their alloys (Pd,[33, 34] Au,[35] Pt[36]) which have proven successful in improving cycle life. For example, Peng et. al. investigated the use of a porous Au cathode (NPG), which allowed a Li-O_2 cell to operate

with 95 % capacity retention after 100 cycles.[37] One of the main reasons behind this excellent performance was the almost exclusive formation of Li_2O_2 upon discharge. That work highlighted the importance of minimizing the formation of parasitic side-products such as LiOH, Li_2CO_3 and HCO_2Li, which are commonly observed for the vast majority of possible electrolytes in the operational voltage window of the cell, typically between 2 - 4.5 V vs Li/Li^+. Another key consideration in Li-O_2 battery operation is the morphology, size, and crystallinity of the Li_2O_2 formed on the cathode as this plays a key role in the charging process (i.e. in Li_2O_2 decomposition).[12, 38] A recent report by Aetukuri et al. examined the impact of H_2O content and Gutman donor/acceptor number (DN and AN) of the electrolyte on the formation of Li_2O_2 for various cathode systems.[39] Their results showed that the formation of commonly noted Li_2O_2 toroids on the cathode surface is promoted by solvents with high DN and/or AN, or due to the presence of H_2O in the electrolyte. Solvents with high DNs are able to stabilize Li^+ species while those with high ANs can stabilize O_2^-, allowing toroid formation which originates in the electrolyte solution. Similarly, it has also been shown that the humidity of ambient air strongly influences the performance of Li-air batteries (i.e. 'open' system architectures) by determining the morphology of Li_2O_2 formed during discharge (enhanced side reactions are also possible).[40-42]

Numerous candidate electrolytes (e.g. tetraglyme,[43-45] sulfolane[46] and N,N-Dimethylacetamide[47]) have been proposed to replace previously used carbonate based electrolytes for Li-O_2 applications. While these electrolytes have all showed enhanced stability in certain cases, the issue of electrolyte stability cannot be considered in isolation as a 'stable' electrolyte for one cathode may be unstable in contact with another cathode. This was clearly shown in the aforementioned report by Peng where a DMSO based electrolyte was found to facilitate stable performance for the NPG cathode but showed rapid decomposition when combined with a carbon based cathode. Furthermore, the long term

suitability of DMSO as electrolyte solvent was very recently called into question by Kwabi et al. who showed that Li_2O_2 reacts with DMSO over extended time periods to form LiOH on the cathode surface.[48] The identification of more stable electrolyte/cathode systems and greater understanding over decomposition mechanisms for electrolytes for different cathodes will likely be a key determinant in the future success of Li-O_2 battery technology.

MnO_2 is a particularly widely studied (electro)catalyst material for Li-O_2 cathodes due to its low cost and ease of fabrication in a variety of morphologies.[49-51] Additionally, its reported bifunctionality with respect to the OER and ORR may actually remove the requirement for supporting carbons given the recent development of other 'carbon free' cathode systems such as Co_3O_4 and TiC.[30, 52-54] While several studies have assessed the impact of MnO_2 catalysts on Li-O_2 battery performance,[24, 27, 50, 55] little information exists on the nature of the discharge products that form compared to those commonly seen for carbon based cathodes. For carbon cathodes, discharge products have been extensively analysed with reports of specific morphologies for Li_2O_2 varying from thin films[56] to spheres[52, 57] and toroids.[58-62] Furthermore, for carbon based cathodes, the morphology of Li_2O_2 formed has been reported to be strongly influenced by the applied current.[56] Similar information on the nature of discharge products formed using MnO_2 based cathodes is lacking and is fundamentally important given the promise of MnO_2 as a bifunctional catalyst.

In this study, we have compared the electrochemical behaviour of MnO_2 nanorods and Super P carbon within a sulfolane based electrolyte. Cathodes composed of pure MnO_2 nanorods (on stainless steel (SS) current collectors) were first investigated electrochemically within an O_2 atmosphere in a split cell configuration using galvanostatic tests. Structural characterization of the morphology of discharge products was performed using electron microscopy. This data was compared with cathodes composed of Super P carbon under identical conditions. A specifically different yet characteristic morphology was found for

each of the discharge products on cathodes with and without MnO_2, and has important implications for the understanding of Li-O_2 battery operation. We show that the lamellar discharge products for MnO_2 form pseudo-spherical layered agglomerates (which are largely insensitive to applied current) while the discharge products for carbon cathodes (which are far more sensitive to current) showed smaller toroidal or spherical particles with increasing proliferation at lower applied current. The nature of the discharge products formed in sulfolane is indicative of high water content in the sulfolane electrolyte but may also suggest decomposition of the electrolyte by the cathode to form water. Pure MnO_2 and Super P based cathodes were also discharged in anhydrous DMSO electrolytes to gauge the impact of water in determining the corresponding discharge product morphology.

Experimental

Materials

Super P carbon and SS meshes were purchased from MTI Corporation USA. Sulfolane (99%), Bis(trifluoromethane) sulfonimide lithium salt (LiTFSI), $MnCl_2.4H_2O$ and PVDF binder were purchased from Aldrich and used as received. Anhydrous DMSO (<5 ppm H_2O) was also purchased from Aldrich and used as received. For tests using DMSO, the LiTFSI salt was dried in a vacuum oven overnight to remove any moisture.

MnO_2 Nanorod Formation

MnO_2 nanorod powders were formed using a modified version of a procedure developed by Chen et al.[49] In a typical reaction, 0.72 g of $MnCl_2.4H_2O$ was mixed in 50 ml isopropanol in a three necked round bottomed flask. The flask was attached to a reflux apparatus and was heated to reflux with constant stirring. While the solution was being heated, 0.4 g of $KMnO_4$

was dissolved in deionized water and stirred to ensure full dissolution. Once the isopropanol solution had reached reflux, the $KMnO_4$ solution was injected into the flask and the temperature was maintained for 10 minutes. The heating mantle was then removed and the solution was allowed to cool to room temperature. The black precipitate was collected by centrifugation and was subsequently washed in deionized water five times. The product was then dried overnight at 80 °C with the resultant solid crushed with a pestle and mortar to form a free flowing powder.

Preparation of Cathodes

All of the cathodes studied were prepared using SS mesh current collector disks from MTI (diameter 1.5 cm, area 1.76 cm^2). All of the active materials investigated were first made up as slurries (with or without binder as specified below) before being dip-coated on to the current collector. Super P slurries were prepared by mixing Super P carbon, PVDF binder and NMP (80:20 weights respectively for the solids). Pure MnO_2 cathodes were made by simply dispersing as-synthesized MnO_2 nanorods in NMP and casting the solution onto SS current collectors. The mixed MnO_2/Super P slurries were made by mixing MnO_2, Super P carbon and PVDF binder (20% of the total MnO_2 + Super P weight) in NMP. All cathodes were dried in an oven overnight at 100 °C to evaporate the NMP solvent and were immediately transferred in to an Ar filled glovebox where they were stored before analysis. Given the importance of mass loading to the operation of Li-O_2 cathodes,[17, 56] the active mass in each case was controlled between 1.4 ± 0.2 mg per cathode unless otherwise stated. As a result, the applied current rate of 100 mAg^{-1} equated to an applied current of 140 ± 20 μA.

Li-O_2 Cell Assembly and Testing

Li-O_2 testing was conducted within an EL-Cell split cell. All cells were constructed within an Ar filled glovebox. Carbon cathodes were first placed on the metal separator. A glass fiber

filter paper was used as separator upon which 100 µl of electrolyte (1M LiTFSI in sulfolane) was placed. A Li chip (MTI) was scraped on both sides and used as the anode. The cell was tightened and removed from the glovebox where it was immediately connected to an O_2 line and was purged with 0.25 bar O_2 for 60 minutes at open circuit voltage (OCV). Following this period, electrochemical measurements were conducted using a VSP Biologic galvanostat. For galvanostatic experiments, the applied current was calculated based on the entire mass of material on the current collector. All voltages quoted are vs Li/Li^+. All capacities are calculated based on the entire mass of the cathode (excluding the weight of the SS current collector).

Material Characterisation

XRD analysis was performed using a Phillips Xpert PW3719 diffractometer using Cu Kα radiation (40 kV and 40 mA) over the range $15° < 2\theta < 70°$. XRD analysis was conducted in air. XRD scans took less than one hour and were conducted on samples which had been stored in the Ar glovebox prior to analysis. We have previously shown that Li_2O_2 formed on Super P cathodes gradually converts to $LiOH.H_2O$ upon air exposure over time (with a complete conversion after 2 weeks).[63] SEM analysis was performed on an FEI Quanta 650 FEG high resolution SEM equipped with an Oxford Instruments X-MAX 20 large area Si diffused EDX detector. Images were collected at an operating voltage of 10-20 kV. All cathodes for SEM analysis were stored in an Ar filled glovebox and transferred in closed containers with 0.1 ppm H_2O and O_2. Samples were loaded into the SEM as rapidly as possible. Karl Fischer titrations were performed using a Metrohm 684 KF coulometer instrument. Samples of the electrolyte were removed from the glovebox in sealed containers and analysed as quickly as possible. The sulfolane based electrolyte showed a H_2O content of approximately ≈2000 ppm (1994 ppm) based on an average of 5 measurements while the

anhydrous DMSO electrolyte contained less than 100 ppm (98 ppm) H_2O (with the majority of the H_2O content likely due to incomplete drying of the LiTFSI salt).

Results and Discussion

Pure MnO_2 Cathodes

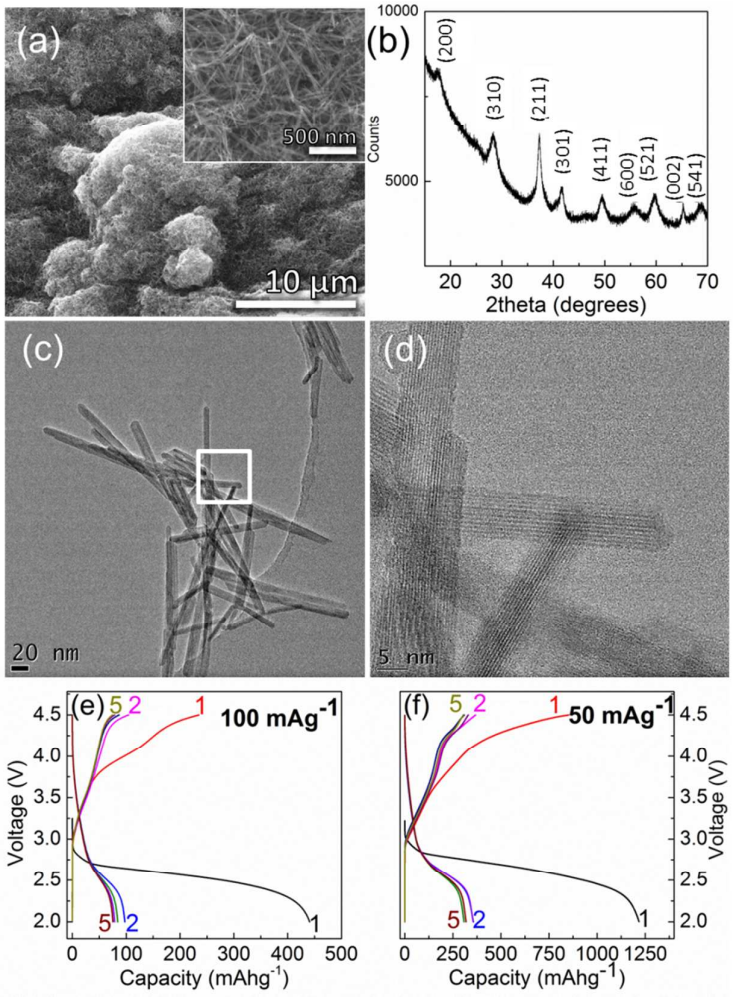

Fig. 1: a) SEM image and magnified inset of pure MnO_2 nanorods as synthesized on SS current collector. b) XRD diffractogram confirming the presence of reflections consistent with the formation of exclusively α-phase MnO_2. c) Low magnification TEM image showing a bundle of MnO_2 nanorods. The high resolution TEM shown in d) was taken from the square region highlighted in c). e) and f) show constant current charge/discharge profiles for 100 mAg^{-1} and 50 mAg^{-1} currents respectively.

MnO_2 nanorods were synthesised according to a scaled-up method first described by Chen et al.[49] Following the synthesis, pure MnO_2 cathodes were made by dispersing the MnO_2 powder in NMP and dip-coating the resultant slurry on to SS mesh current collectors. Cathodes were prepared without the addition of binders. The SEM image presented in Fig. 1 a) is a low magnification image of a MnO_2 cathode with the higher magnification image (inset) clearly showing the morphology of the constituent nanorods and also the highly interconnected nature of the material on the cathode. XRD analysis presented in Fig. 1 b) shows reflections consistent with tetragonal phase α-MnO_2 (space group I4/m) as previously reported and none of the other possible Mn_xO_y phases.[41] TEM analysis revealed that the nanorod diameters were between 5 and 15 nm with associated aspect ratios typically ≈ 20 (Fig. 1 c). HRTEM analysis (Fig. 1 d) confirmed that the all of the nanorods were single crystal while also revealing that the nanorods had rough surfaces. Galvanostatic discharge/charge cycles conducted on the pure MnO_2 cathodes using specific currents of 100 mAg^{-1} (Fig. 1 e)) and 50 mAg^{-1} (Fig. 1 f)) showed initial discharge capacities of 444 $mAhg^{-1}$ and 1219 $mAhg^{-1}$ respectively, with a slight reduction in the discharge overpotential found at lower current density. The average cell potential corresponded to ≈ 2.7 V for 50 mA g^{-1} and 2.6 V for 100 mAg^{-1}. The initial charge capacities for the corresponding currents were 239 $mAhg^{-1}$ and 857 $mAhg^{-1}$. Subsequent discharge/charge cycles showed more modest capacities as often seen in previous studies.

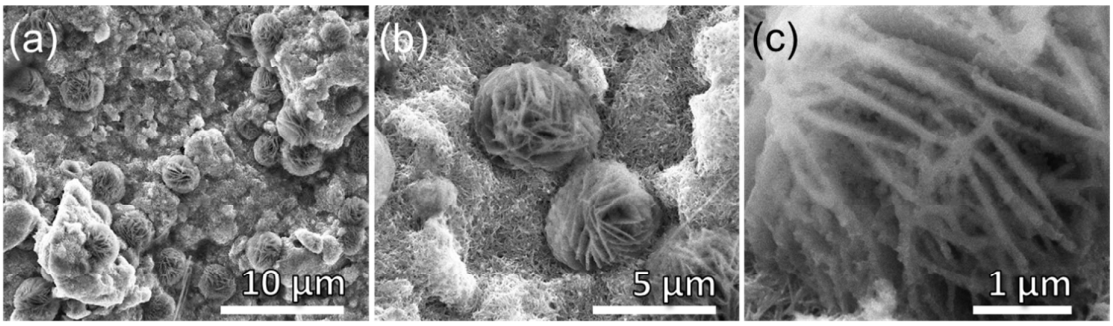

Fig.2: SEM images of a pure MnO_2 cathode discharged at a current rate of 100 mAg^{-1}. There are a number of large agglomerates covering the underlying MnO_2. b) An example of two large plate agglomerates with the interlinked MnO_2 clearly visible in the background. c) High magnification image of single agglomerate.

Ex-situ analyses were carried out on a pure MnO_2 cathode after a single discharge to investigate the formation of discharge products. At an applied current rate of 100 mAg^{-1}, a high density of large agglomerates were formed across the surface of the cathode (Fig. 2 a). These agglomerates were typically less than 5 µm in diameter (Fig. 2b) and formed directly on the underlying MnO_2 nanorods. The layered assembly of the sheets in the agglomerates is shown in Fig. 2 c). Such layered agglomerates have recently been mentioned as the primary discharge product for MnO_2 nanowire based cathodes but were not thoroughly investigated in that study.[28] These large plate agglomerates were found to be air sensitive and structural alterations were observed after being exposure to air for 1 week (SI Fig. S1). This fact, coupled with the high O_2 signal present using EDX analysis (SI Fig. S2) suggests that the structures were composed of either Li_2O_2 or LiOH, however, XRD analysis conducted on the MnO_2 cathodes was not able to identify the presence of any crystalline discharge products (SI Fig. S3). We note that Kwabi et al. recently attributed similar shaped discharge products to LiOH formation from the reaction of Li_2O_2 with DMSO.[48] Similarly, Xu et al. suggested that flake-like particles formed on carbon cathodes using a DMSO electrolyte were composed of LiOH (or $LiOH.H_2O$).[46] Thus, we tentatively attribute these large flake-like agglomerates to

LiOH formed on the MnO_2 based cathodes. The role of the cathode material and electrolyte in determining the composition of discharge products will be discussed in a later section.

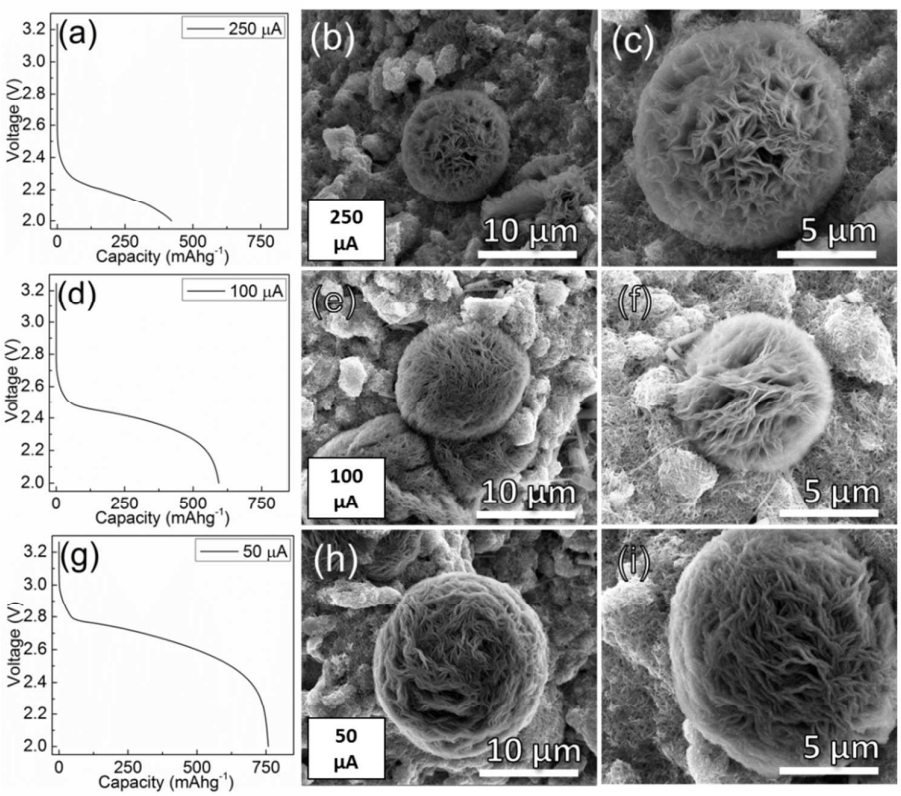

Fig.3: Discharge curves and SEM images of discharge products noted at different applied currents (250 µA (a,b,c), 100 µA (d,e,f) and 50 µA (g,h,i)) for single discharges of pure MnO_2 cathodes.

To further investigate the influence of MnO_2 on the discharge products formed in the first discharge cycle, pure MnO_2 cathodes were subjected to single discharges with applied currents varied from 250-50 µA (Fig. 3 a,d,g respectively). A higher rate test was also conducted with an applied current of 500 µA. However, the first discharge occurred rapidly (~20 mins) and no discharge products were noted when the cathode was analysed using SEM (SI Fig. S4). In contrast, tests run at lower currents showed clear discharge product formation across the cathode surfaces. In Fig. 3 (b,c) characteristic agglomerates similar to those noted in Fig. 2 (albeit slightly more spherical) are visible on the cathode subjected to a discharge at

an applied current of 250 μA. Similarly, highly layered agglomerates were also noted at lower currents (Fig. 3 (e,f) 100 μA and Fig. 3 (h,i) 50 μA) with the majority being pseudo-spherical (additional examples of discharge products at each of these applied current can be seen in SI Fig. S5). The morphology of these discharge products was found to be largely independent to the applied current with a change to much larger agglomerates (greater than 20 μm in size in some cases) only noted at applied currents of 10 and 25 μA (SI Fig. S6).

Pure Super P Carbon Cathodes

As a direct comparison with pure MnO_2 cathodes, slurry-based Super P carbon cathodes were produced and analysed. These measurements were conducted with similar mass loadings to those analysed for MnO_2 (1.4 ± 0.2 mg per cathode) meaning that there was a much larger surface area for the carbon cathodes. Apart from the difference in volume of active materials between the MnO_2 and Super P cathodes, all other parameters in the tests were identical (anode, electrolyte, cell architecture etc.).

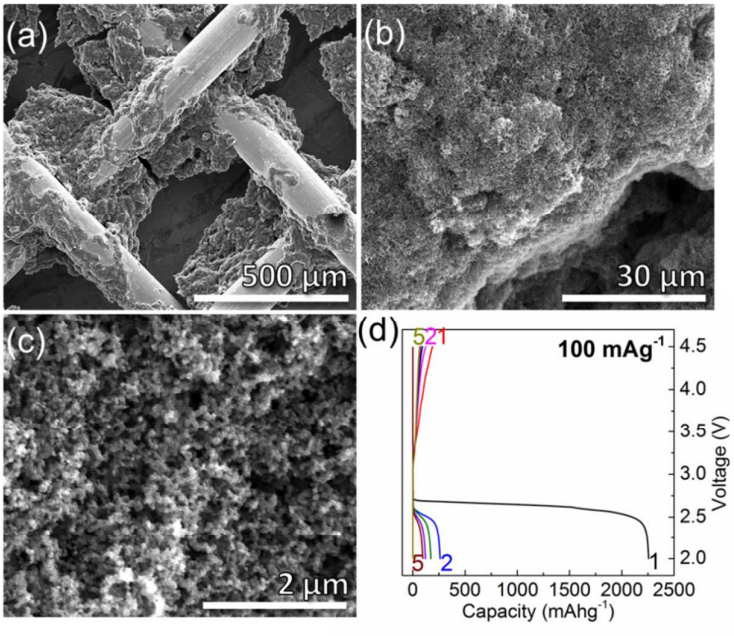

Fig. 4: a)-c) SEM images of pristine Super P carbon cathodes on SS mesh current collector. d) Charge/discharge profiles for 5 cycles obtained with an applied current of 100 mAg^{-1} .

Fig. 4 a)-c) are SEM images at progressively higher magnifications showing the nature of the pristine Super P carbon on the SS mesh current collector. The particle size and packing is consistent with those previously noted for Super P cathodes which are known to possess high surface area and good O_2 transfer ability.[64] Galvanostatic analysis performed at a specific current of 100 mAg^{-1} show a high initial discharge capacity of 2250 $mAhg^{-1}$ (based on the entire mass of cathode material including PVDF binder) with a far more modest initial charge capacity of circa 225 $mAhg^{-1}$. Similar to MnO_2 cathodes in a sulfolane electrolyte, the average cell potential on the initial discharge is also 2.6 V – 2.7 V. A negligible change in overpotential for Li_2O_2 formation is observed, yet a marked reduction in the full cycle efficiency is noted compared to MnO_2 electrodes. Subsequent discharge and charge cycles never exhibited high capacities.

SEM analysis performed on a Super P cathode after a single discharge at a current rate of 100 mAg^{-1} showed completely different morphologies for the discharge products when compared to those seen for MnO_2 cathodes at the same rate without a reduction in cell potential. Pseudo-spherical, toroidal particles (SI Fig. S7) were noted across the surface of the cathode which is consistent with observations from previous SEM studies on the discharge products formed upon pure carbon cathodes.[59, 61, 65] The formation of toroids also reflects the high water content of the sulfolane electrolyte which was measured by Karl-Fischer titration to be ≈2000 ppm. It has clearly been shown by Aetukuri et al. that the formation of toroidal Li_2O_2 particles is favoured in H_2O containing electrolytes.[39] The discharge products observed are in stark contrast to those noted for the pure MnO_2 cathodes. First, they tend to be almost an order of magnitude smaller in size (approximately 500 nm and 5 μm on the Super P and MnO_2 cathodes, respectively). Second, their morphology is characteristically toroidal compared to layered flake agglomerates on MnO_2. Additionally, XRD analysis of the cathode

after single discharge (SI Fig. S8) showed clear evidence of the formation of crystalline Li_2O_2 on the cathode surface. This shows that the experimental setup was capable of identifying crystalline Li_2O_2 on the carbon based cathodes. However, it does not rule out the possibility of the formation of amorphous by-products on the cathodes.

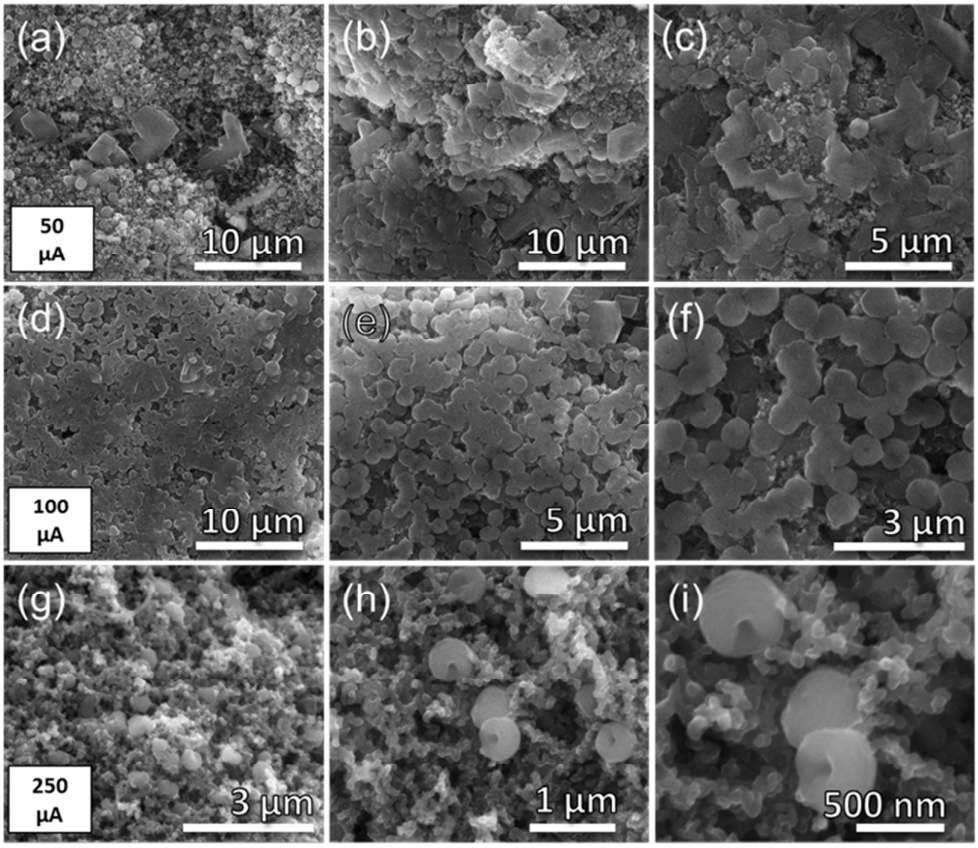

Fig. 5: SEM images of singly discharged Super P cathodes at 50 µA(a-c), 100 µA (d-f) and 250 µA (g-i).

Single discharges were also conducted for pure Super P cathodes at the same applied currents as those examined in Fig. 3 for MnO_2 cathodes (discharge profiles are shown in SI Fig. S9). The nature of the discharge products was found to be more strongly dependent upon the applied current than for the MnO_2 cathodes. For the discharges at 50 and 100 µA applied current, the cathodes showed a large quantity of Li_2O_2 formed across their entire surface. For

the 50 μA cathode (Fig. 5 a-c)), the surface of the underlying carbon can be seen to be widely covered by a film of Li_2O_2 with evidence that the film is composed of fused toroids. After full discharge at 100 μA applied current (Fig. 5 d-f) we note a widespread Li_2O_2 film formation on the carbon surface (Fig. 5 d) and a pronounced fusion of circular particles (Fig. 5 e,f). The corresponding discharge profiles show a higher average potential for oxygen reduction at the carbon electrode which occurs together with widespread filming by electrically passivating Li_2O_2. At an applied current of 250 μA, the nature of the discharge product was markedly different (Fig. 5 g-i). No evidence of Li_2O_2 film formation was noted with the discharge product instead existing as mostly isolated toroids across the carbon surface. Additional examples at each current rate can again be found in SI Fig. S10 while SEM images of Super P cathodes discharged at 10 μA, 25 μA and 175 μA are shown in SI Fig. 11. The morphologies of the discharge products for Super P cathodes and MnO_2 cathodes discharged in sulfolane in this study are summarized in Table 1.

Table 1: Summary of the various morphologies formed on MnO_2 and Super P cathodes in sulfolane electrolyte

Current / Cathode	10 μA	25 μA	50 μA	100 μA	175 μA	250 μA
MnO_2	Very large non-spherical flake agglomerated layered structures >20 μm in size	Very large non-spherical flake agglomerated layered structures >20 μm in size	Pseudo spherical flake agglomerates <10 μm in size with thicker plates and some agglomeration	Pseudo spherical flake agglomerates <10 μm in size (some fusion or agglomerates noted)	Pseudo spherical flake agglomerates <10 μm in size	Pseudo spherical flake agglomerates <10 μm in size
Super P	Widespread fused particles (250 nm→1 μm)	Widespread fused large particles (250 nm→1 μm)	Fused toroids and larger sheets	Widespread fused toroids and particles	Isolated toroids and larger particles (500 nm→1 μm)	Isolated toroids (circa 400 nm)

Mixed Super P/MnO_2 Cathodes

The majority of studies investigating MnO_2 nanorods for use as Li-air battery catalysts to date have focused on MnO_2/carbon composites.[26] To reflect this, mixed MnO_2/Super P cathodes were made by mechanically mixing MnO_2 nanorods with Super P carbon. Despite the fact that the MnO_2 nanorods were mixed with the Super P overnight, segregation of the MnO_2 into clumps was noted using SEM analysis (SI Fig. S12).

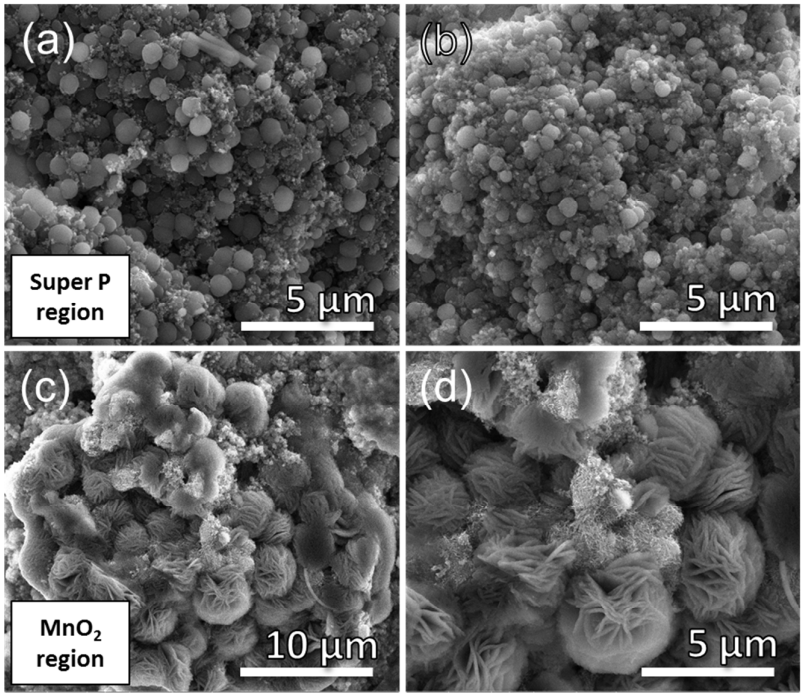

Fig. 6: SEM images of the discharge products formed on one 50% MnO_2/Super P cathode at an applied current of 250 µA. Due to segregation of the MnO_2 nanorods the Super P only regions showed only toroidal particles (a,b) while the MnO_2 nanorod covered regions showed characteristic flake agglomerates (c,d).

To probe the nature of the discharge production morphology differences and segregation on mixed MnO_2/Super cathodes, a single discharge was performed on a 50% MnO_2/Super P cathode with an applied current of 250 µA. During discharge tests with the Super P cathode (cf. Fig. 5) at this current (250 µA), isolated toroids are formed, which improves the accuracy of alternative discharge product identification and segregation on

MnO_2 portions of the mixed cathode surface. As previously noted, these cathodes exhibited some inhomogeneity with large clumps of MnO_2 nanorods present on the cathode surface. As shown in Fig. 6, strikingly different morphologies are noted for discharge products across a single cathode surface. In the areas with only Super P carbon, characteristic toroidal Li_2O_2 particles were noted in high density (with no visible particle fusing or thin film formation). Large spherical flake agglomerates were also noted across the cathode surface either singly or in bundles as seen in Fig. 6 c,d) (see Fig. S13 for more examples). Each of these characteristic aggregates was found to be either resting on, or interspersed with, large bundles of MnO_2 nanorods. This result shows conclusively that the host cathode material plays a crucial role in determining the nature of the discharge products formed on the cathode surface (even within a single cathode). Since these large flake agglomerates are likely composed of LiOH, the discharge product density, phase and morphology segregation suggest that MnO_2 actively promotes the formation of LiOH. In this case, LiOH is formed rather than Li_2O_2 in electrolytes that contain H_2O or can form H_2O from catalytic decomposition of H_2O_2 formed in the presence of PVDF, with O^{2-} constituting the H-abstraction species to initiate this process.[66] Under identical discharge and cell conditions within the same cathode, Li_2O_2 however, is still confirmed to form on the carbon portion of the same cathode, and on pure carbon cathodes.

Anhydrous DMSO as Electrolyte Solvent

Additional tests were carried out using anhydrous DMSO as the electrolyte solvent to gauge the impact of H_2O in determining the electrochemical response. A single discharge was conducted on a MnO_2 cathode (free of PVDF binder and with similar mass loading to the tests conducted with sulfolane electrolyte) at a current of 50 μA (Fig. 7a). This current was chosen as it had previously led to the widespread formation of flake agglomerates across the cathode surface for the sulfolane tests. It was noted that the discharge capacity for the MnO_2

cathode was similar to that observed for the singly discharged sulfolane cathode presented in Fig. 3g). As can be seen in the SEM images presented in Fig. 7(b-d), large flake agglomerates of similar sizes and areal coverage were identified across the MnO_2 cathode surface. The density, size and morphology were very similar to that found in H_2O-containing sulfolane electrolyte.

To explain the appearance of the large flake agglomerates (which are most likely composed of LiOH) on both the MnO_2 cathodes discharged in anhydrous and H_2O containing sulfolane, it is worth noting that several pathways exist for LiOH formation. Trahan et al. proposed that LiOH formation on Li-O_2 battery cathodes in the presence of a DMSO electrolyte can be caused by superoxide anions acting as a base to remove the weakly acidic protons of DMSO according to eq 1.[67] LiOH can then be formed in solution according to eq 2.[67] Alternatively, LiOH can also be formed directly from H_2O by reaction with Li_2O_2 according to eq 3 as shown by Black et al.[66] When considering the apparent formation of LiOH on the cathode discharged in anhydrous DMSO, it is clear that the primary source of LiOH should be due to reactions between the superoxide anions and DMSO as shown in eq 1 followed by the reaction in eq 2 to form LiOH, since H_2O formation via decomposition of H_2O_2 that requires H_2O formation from dehydrofluorinated PVDF reactions with LiO_2 can be eliminated. LiOH formation can be proposed due to the reactivity of DMSO with superoxide anions and the lack of inherent water content in the electrolyte.

Eq 1: $CH_3SOCH_3 + O_2^- \rightarrow CH_3SOCH_2^- + H_2O$

Eq 2: $H_2O + Li^+ + e^- \rightarrow LiOH + ½\ O_2$

Eq 3: $Li_2O_2 + 2H_2O \rightarrow 2LiOH + H_2O_2$

Conversely, the formation of LiOH on cathodes discharged in the water-containing sulfolane is slightly more complex. It is unclear whether the sulfolane electrolyte is prone to decomposition by O_2^- in the same manner as DMSO or whether the inherent water in the sulfolane reacts with Li_2O_2 to form LiOH. This may be a possibility given that the sulfolane electrolyte has been shown to be capable of forming solution mediated Li_2O_2 toroids (Fig. 5) on carbon surfaces.

In pure MnO_2 cathodes (C- and PVDF-free) in both electrolytes, a unique morphology of LiOH is formed. We posit that conversion of Li_2O_2 (from solution in the case of H_2O-containing electrolytes) to LiOH may occur specifically when deposited onto the surface. The unique morphology is thus a likely consequence of further nucleation of self-similar phases at these segregated MnO_2 regions. In the mixed cathode however, the presence of PVDF provides additional side-reactions summarized in Eq 4 that lead to LiOH by effective catalytic formation of *in-situ* formed H_2O_2 to H_2O during its disproportionation reaction. It is not clear if this process may dominate over other reactions involving superoxide anions and DMSO; in both cases H_2O is formed, but the former case is more specific to MnO_2 since it is an excellent H_2O_2 decomposition catalyst.[68] Furthermore, if the PVDF-mediated formation of H_2O that converted Li_2O_2 to LiOH occurs uniquely at the MnO_2 regions, more H_2O_2 would be formed from Eq 3 that would result in a continuous process that depends on the amount of MnO_2 surface and the reactants involved in H_2O production.

Eq 4: $H_2O_2 \rightarrow H_2O + ½\ O_2$

LiOH likely forms from reaction of Li_2O_2 with water, suggesting Li_2O_2 does form on MnO_2 surfaces, or LiOH nucleates on MnO_2 surfaces preferentially from reaction of solution-borne Li_2O_2 to LiOH that subsequently precipitates on the oxide surface. The segregation and

unique morphology difference between MnO_2 and carbon surface (Fig. S13), in each electrolyte (wet or dry), is one outcome of the suggested mechanism.

Filming or coverage of carbon by poor electron conducting Li_2O_2 limits electrochemical cross-talk between Li_2O_2 species on carbon and MnO_2, blocking further electrocatalytically driven reaction to mimic what occurs at the MnO_2 surface. With segregated 'catalyst' and carbon regions, the process on each respective surface rea unique to those surfaces and the MnO_2 does not seem to influence the discharge process of the cathode as a whole. Thus, uniform mixing is necessary to invoke a unique or dominant discharge process in metal oxide-containing carbon Li-O_2 cathodes. Even still, the presence of the other material has limited benefit except to increase cathode mass. We suggest that in sulfolane and DMSO, regardless of inherent H_2O content, LiOH will result if MnO_2 catalysts are used; it will still form in anhydrous DMSO with mixed cathodes that contain PVDF. Thus, the unique segregation and morphology of the discharge products on MnO_2 are symptomatic of specific surface growth caused by *in-situ* H_2O formation in wet sulfolane electrolytes, or from reaction with anhydrous DMSO to form H_2O, or indeed from PVDF-mediated reactions in the case of mixed cathodes formed with a F-containing binder in either electrolyte. In this later case, the quantity of H_2O generated is likely to be the greatest and thus LiOH species can also be found on carbon surfaces from reaction with Li_2O_2.

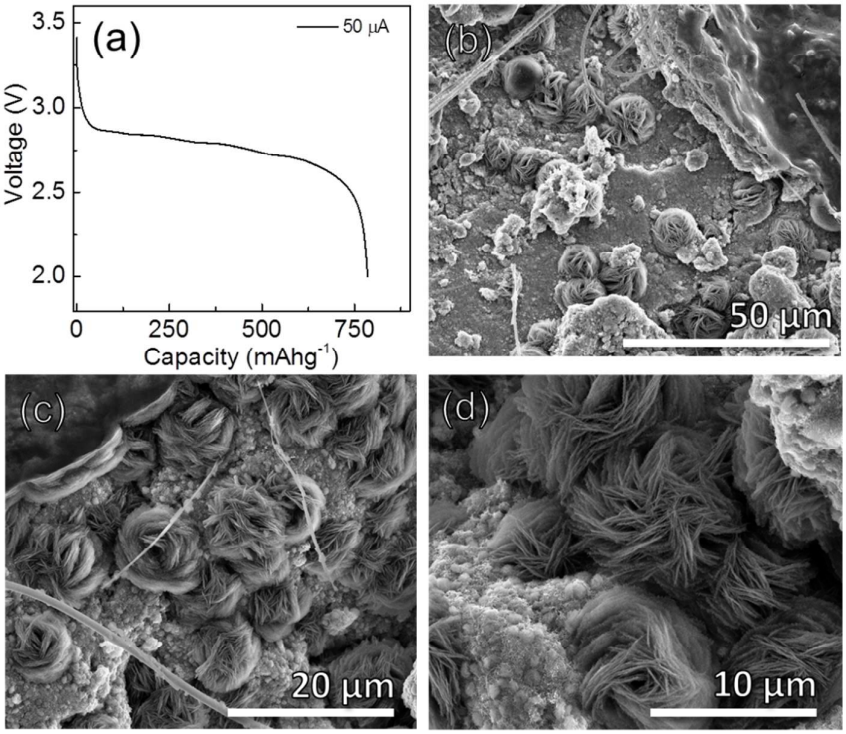

Fig. 7: a) Discharge curve of MnO_2 cathode in anhydrous DMSO electrolyte. b-d) SEM images at increasing magnification of the discharged cathode showing the formation of large agglomerates on the cathode surface.

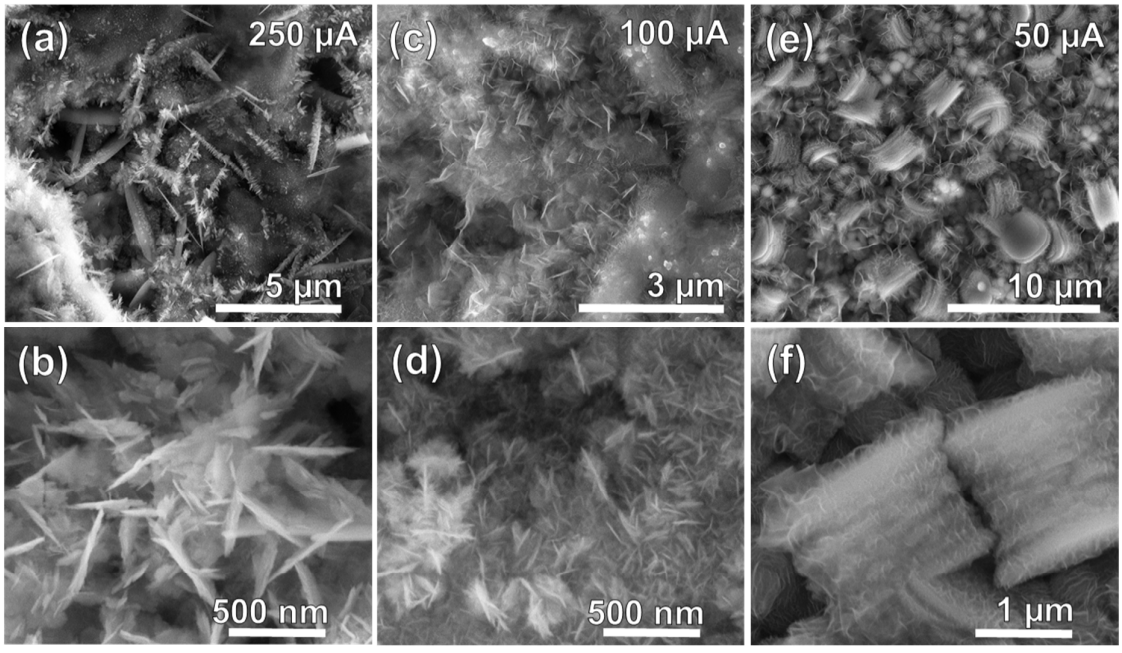

Fig 8: SEM images of Super P carbon cathodes discharged in anhydrous DMSO at various applied currents ((a,b) 250 μA (c,d) 100 μA (e,f) 50 μA).

Super P cathodes containing PVDF binder discharged (See SI Fig. 14 for discharge profiles) in anhydrous DMSO showed radically different discharge products to those observed for sulfolane discharged cathodes. At high currents (Fig 8 a,b), only thin sheet-like discharge products were noted across the cathode surface, with similar discharge products formed at 100 μA. At an applied current of 50 μA (Fig 8 e,f) much larger agglomerates were observed. No toroids were present on the carbon cathode surface at any of the applied currents in anhydrous DMSO. XRD analysis of the cathode discharged at 100 μA (SI Fig. S15) showed the presence of crystalline Li_2O_2 but also $LiOH.H_2O$. The presence of PVDF in the Super P cathode may be the cause of this by-product. Its enhanced reactivity with DMSO compared to sulfolane was previously highlighted.[46] As noted previously, neither LiOH nor $LiOH.H_2O$ were observed using XRD for the Super P cathode discharged in sulfolane (SI Fig S8); Li_2O_2 was detected as the sole crystalline discharge product in that case. Despite this, Super P cathodes showed much better cycling behaviour in DMSO compared to sulfolane (SI Fig. 16). The initial discharge capacity was ≈1600 $mAhg^{-1}$ with >70 % capacity retention at the fifth discharge cycle. The onset of charging in DMSO was found to be much lower compared to the sulfolane at ≈ 3.75 V. This reduction in overpotential may be due to the difficulty in decomposing the large Li_2O_2 toroids formed upon charge in sulfolane compared to the smaller discharge products formed in DMSO.[38] In all dedicated tests in anhydrous DMSO, and H_2O-containing sulfolane, the formation of LiOH is specific to electrolyte *and* cathode formulation. We note that LiOH itself has been reported to decompose DMSO over long periods, with the formation of H_2O and other species (methylsulfonates and sulphites)[60], its decomposition during discharge is not clearly observed. For MnO_2-containing cathodes, the specific formation of LiOH may influence the charging characteristics in Li-O_2 systems.

Proton abstraction mechanisms that results in further side reactions have been proposed by Sharon *et al*. for surface-bound LiOH species after discharge, and our work shows how this phase is preferably formed in wet electrolytes, on MnO_2 cathodes, and how its formation is further promoted by *in-situ* generated H_2O during discharge.

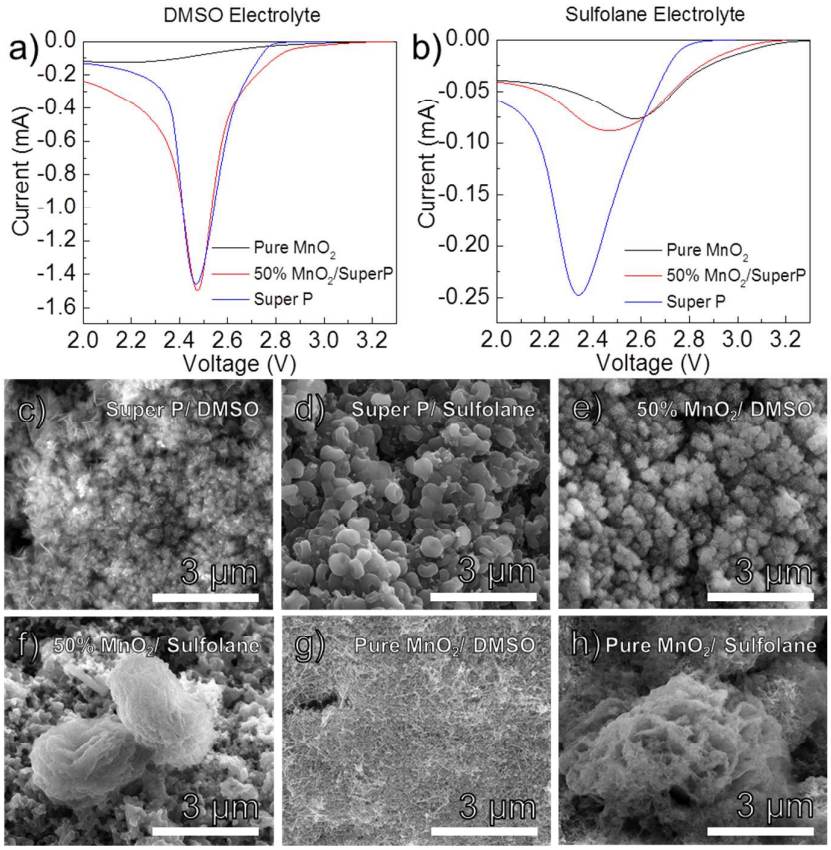

Fig 9: Linear voltage sweeps of pure MnO_2, 50% MnO_2/Super P and Super P cathodes in a) DMSO electrolyte and b) Sulfolane electrolyte at a scan rate of 0.05 mV/s c-h) Corresponding SEM images after the linear voltage tests.

Linear voltage sweeps were conducted on cathodes composed of Super P, 50% MnO_2/Super and pure MnO_2 in DMSO (Fig. 9 a) and Sulfolane (Fig. 9 b) with the corresponding SEM images for the different cathodes shown in Fig 9 (c-h). A characteristic cathodic current peak is observed, and the peak potential and total integrated area (charge) are found to vary for the Super P cathodes in the two electrolytes. For DMSO, a sharp peak

centred at ≈ 2.45 V was noted compared to a broader, more asymmetric peak centred at ≈ 2.35 V for sulfolane. Comparing the morphologies of the respective discharge products, it can be seen that small flake-like products were noted in DMSO ((Fig 9 c) similar to Fig 8), while characteristic Li_2O_2 toroids were formed in sulfolane ((Fig 9 d) similar to those presented in Fig 5). The cathodic profile and potential of the peaks associated with the product formation are consistent with recent observations by Aetukuri et al. who showed that toroid formation tends to occur via a solution mediated process at lower voltages compared to surface driven growth (which occurs at higher voltages) in similar linear voltage sweep tests.[39] In that work, the peak and its potential were related to solution and surface-mediated Li_2O_2 formation, although other phases form as demonstrated here.

The cathodes containing MnO_2 showed different responses in the two electrolytes. For DMSO, the pure MnO_2 test showed a broad response at lower voltages compared to the Super P (centred at 2.2 V) while the voltage sweep in sulfolane in contrast was higher compared to the Super P and was centred at 2.6 V. This different electrochemical response is tentatively attributed to the initial presence of H_2O in the sulfolane and absence in DMSO but will be the subject of further investigations. When comparing the SEM images of the pure MnO_2 cathodes, there was no obvious wide-scale discharge product formation noted in the case of DMSO (Fig. 9 g) while for sulfolane (Fig. 9 h), large agglomerates were noted. For the 50% Super P/ MnO_2 cathodes, it can be seen that the potentials and cathodic peak profiles of the voltage sweeps are shifted to more positive potentials compared to the pure Super P cathodes by the presence of the MnO_2. In sulfolane, large agglomerates were observed across the cathode surface (Fig. 9 f) while the majority of the discharge products for the DMSO cathode were small flakes consistent with the pure Super P cathode.

Conclusions

We have investigated the impact of MnO_2 nanorod catalysts on the electrochemical response within Li-O_2 battery cathodes in two electrolyte systems (water containing sulfolane and anhydrous DMSO). By directly comparing pure MnO_2 cathodes to those composed of Super P carbon in both systems, the direct influence of MnO_2 on the discharge process, characteristics and products was obtained. The nature of the discharge products formed at various applied currents was compared for both types of cathodes. Each cathode showed specifically different discharge product morphologies based on the cathode material and electrolyte used. Large flake agglomerates (most likely composed of LiOH) formed on MnO_2 in both electrolytes suggesting that MnO_2 actively promotes side reactions in both electrolytes from the first discharge. The deterministic role of MnO_2 in catalysing side reactions not related to ORR or Li_2O_2 formation was further demonstrated by the fact that the characteristic LiOH flake agglomerates were noted only on MnO_2 surfaces, even when discharges were conducted with mixed carbon/MnO_2 cathodes. In such cases, even with H_2O and PVDF constituents in the S-containing electrolytes, Li_2O_2 formation was found segregated to the carbon surface.

In contrast, smaller toroids, particles and thin films were formed on the Super P carbon cathodes discharged in sulfolane while flake like discharge products were noted on carbon cathodes discharge in anhydrous DMSO. XRD analysis suggests only Li_2O_2 as the crystalline discharge product on sulfolane discharged carbon cathodes, while additional reflections consistent with LiOH.H_2O were noted for DMSO. These results give further insight into the complex chemistry associated with Li-O_2 battery operation and the importance of identifying compatible electrolyte/cathode pairings. In some cathode formulations, the use of typical electrocatalytic material does enhance reactivity, but not always for the reversible phase required for high coulometric efficiency operation of the

battery. When mechanisms that form *in-situ* H_2O and associated reactions govern the primary discharge process, true reversibility in MnO_2 containing carbon cathodes may be hampered by the formation of unwanted LiOH species in sulfolane and DMSO. The work highlights the importance of factors governing *in-situ* and electrochemically generated water content of electrolytes in determining the nature of Li_2O_2 and LiOH phases formed on carbon cathodes, and the care in the choice of (electro)catalyst and polymer binder in Li-O_2 cathodes to avoid promoting side reactions on the surface and in the electrolyte solution.

Author Information

To whom correspondence should be addressed: Email: c.odwyer@ucc.ie; Tel: (0)21 4902732; Fax: (0)21 4274097

Acknowledgements

This research has received funding from the Seventh Framework Programme FP7/2007-2013 (Project STABLE) under grant agreement n°314508. Support from the Irish Research Council New Foundations Award is also gratefully acknowledged. HG would like to thank Dr. Subhajit Biswas for assistance with EDX analysis.

Supporting Information

EDX analysis of discharge products formed on MnO_2 cathodes, additional discharge profiles for MnO_2 and Super P cathodes and additional SEM images of Super P and MnO_2 cathodes and associated discharge products.

References

1. Li, Y.; Huang, Z.; Huang, K.; Carnahan, D.; Xing, Y. *Energy Environ. Sci.* **2013,** 6, (11), 3339-3345.
2. Cao, R.; Lee, J.-S.; Liu, M.; Cho, J. *Adv. Energy Mater.* **2012,** 2, (7), 816-829.
3. Lee, J.-S.; Tai Kim, S.; Cao, R.; Choi, N.-S.; Liu, M.; Lee, K. T.; Cho, J. *Adv.Energy Mater.* **2011,** 1, (1), 34-50.
4. Li, F.; Zhang, T.; Zhou, H. *Energy Environ. Sci.* **2013,** 6, (4), 1125-1141.
5. Bruce, P. G.; Freunberger, S. A.; Hardwick, L. J.; Tarascon, J. M. *Nature Mater.* **2011,** 11, (1), 19-29.
6. Bhatt, M. D.; Geaney, H.; Nolan, M.; O'Dwyer, C. *Phys. Chem. Chem. Phys.* **2014,** 16, (24), 12093-12130.
7. Li, L.; Chai, S.-H.; Dai, S.; Manthiram, A. *Energy Environ. Sci.* **2014**, 7, 2630-2636

8. Li, L.; Zhao, X.; Fu, Y.; Manthiram, A. *Phys. Chem. Chem. Phys.* **2012,** 14, (37), 12737-12740.
9. Abraham, K.; Jiang, Z. *J. Electrochem. Soc.* **1996,** 143, (1), 1-5.
10. Wang, J.; Li, Y.; Sun, X. *Nano Energy*, **2013**, 2, 443–467
11. Jung, H.-G.; Hassoun, J.; Park, J.-B.; Sun, Y.-K.; Scrosati, B. *Nature Chem.* **2012,** 4, (7), 579-585.
12. Gallant, B. M.; Kwabi, D. G.; Mitchell, R. R.; Zhou, J.; Thompson, C.; Shao-Horn, Y. *Energy Environ. Sci.* **2013**, 6, 2518-2528
13. Read, J. *J. Electrochem. Soc.* **2002,** 149, (9), A1190-A1195.
14. Gallagher, K. G.; Goebel, S.; Greszler, T.; Mathias, M.; Oelerich, W.; Eroglu, D.; Srinivasan, V. *Energy Environ. Sci.* **2014**, 7, 1555-1563
15. Christensen, J.; Albertus, P.; Sanchez-Carrera, R. S.; Lohmann, T.; Kozinsky, B.; Liedtke, R.; Ahmed, J.; Kojic, A. *J. Electrochem. Soc.* **2011,** 159, (2), R1-R30.
16. Garcia-Araez, N.; Novák, P. *J. Solid State Electrochem.* **2013**, 1-15.
17. Beattie, S.; Manolescu, D.; Blair, S. *J. Electrochem. Soc.* **2009,** 156, (1), A44-A47.
18. Mirzaeian, M.; Hall, P. J. *Electrochimica Acta* **2009,** 54, (28), 7444-7451.
19. Ottakam Thotiyl, M. M.; Freunberger, S. A.; Peng, Z.; Bruce, P. G. *J. Am. Chem. Soc.* **2013,** 135, (1), 494–500
20. Itkis, D. M.; Semenenko, D. A.; Kataev, E. Y.; Belova, A. I.; Neudachina, V. S.; Sirotina, A. P.; Hävecker, M.; Teschner, D.; Knop-Gericke, A.; Dudin, P.; Barinov, A.; Goodilin, E. A.; Shao-Horn, Y.; Yashina, L. V. *Nano Lett.* **2013,** 13, (10), 4697-4701.
21. McCloskey, B. D.; Bethune, D. S.; Shelby, R. M.; Girishkumar, G.; Luntz, A. C. *J. Phys. Chem. Lett.* **2011,** 2, (10), 1161-1166.
22. McCloskey, B. D.; Speidel, A.; Scheffler, R.; Miller, D. C.; Viswanathan, V.; Hummelshøj, J. S.; Nørskov, J. K.; Luntz, A. C. *J. Phys. Chem. Lett.* **2012,** 3, (8), 997-1001.
23. Shao, Y.; Park, S.; Xiao, J.; Zhang, J.-G.; Wang, Y.; Liu, J. *ACS Catal.s* **2012,** 2, (5), 844-857.
24. Truong, T. T.; Liu, Y.; Ren, Y.; Trahey, L.; Sun, Y. *ACS Nano* **2012,** 6, (9), 8067-8077.
25. Débart, A.; Paterson, A. J.; Bao, J.; Bruce, P. G. *Angew. Chem.* **2008,** 120, (24), 4597-4600.
26. Qin, Y.; Lu, J.; Du, P.; Chen, Z.; Ren, Y.; Wu, T.; Miller, J. T.; Wen, J.; Miller, D. J.; Zhang, Z.; Amine, K. *Energy Environ. Sci.* **2013,** 6, (2), 519-531.
27. Cheng, H.; Scott, K. *J. Power Sources* **2010,** 195, (5), 1370-1374.
28. Song, K.-S.; Jung, J.; Heo, Y. U.; Lee, Y. C.; Cho, K.; Kang, Y. *Phys. Chem. Chem. Phys.* **2013**, 15, 20075-20079
29. Guo, Z.; Zhu, G.; Qiu, Z.; Wang, Y.; Xia, Y. *Electrochem. Commun.* **2012,** 25, (0), 26-29.
30. Riaz, A.; Jung, K.-N.; Chang, W.; Lee, S.-B.; Lim, T.-H.; Park, S.-J.; Song, R.-H.; Yoon, S.; Shin, K.-H.; Lee, J.-W. *Chem. Commun.* **2013**, 49, 5984-5986
31. Kong, F. *Electrochimica Acta* **2012,** 68, 198-201.
32. Park, C. S.; Kim, K. S.; Park, Y. J. *J. Power Sources* **2013,** 244, (0), 72-79.
33. Shen, Y.; Sun, D.; Yu, L.; Zhang, W.; Shang, Y.; Tang, H.; Wu, J.; Cao, A.; Huang, Y. *Carbon* **2013,** 62, (0), 288-295.
34. Zhu, D.; Zhang, L.; Song, M.; Wang, X.; Chen, Y. *Chem. Commun.* **2013**,49, 9573-9575
35. Lu, Y.-C.; Xu, Z.; Gasteiger, H. A.; Chen, S.; Hamad-Schifferli, K.; Shao-Horn, Y. *J. Am. Chem. Soc.* **2010,** 132, (35), 12170-12171.
36. Lim, H.-D.; Song, H.; Gwon, H.; Park, K.-Y.; Kim, J.; Bae, Y.; Kim, H.; Jung, S.-K.; Kim, T.; Kim, Y. H.; Lepro, X.; Ovalle-Robles, R.; Baughman, R. H.; Kang, K. *Energy Environ. Sci.* **2013,** 6, (12), 3570-3575.
37. Peng, Z.; Freunberger, S. A.; Chen, Y.; Bruce, P. G. *Science* **2012,** 337, (6094), 563-566.
38. Hu, Y.; Han, X.; Cheng, F.; Zhao, Q.; Hu, Z.; Chen, J. *Nanoscale* **2014,** 6, (1), 177-180.
39. Aetukuri, N. B.; McCloskey, B. D.; García, J. M.; Krupp, L. E.; Viswanathan, V.; Luntz, A. C. *arXiv preprint arXiv:1406.3335* **2014**.
40. Guo, Z.; Dong, X.; Yuan, S.; Wang, Y.; Xia, Y. *J. Power Sources* **2014,** 264, (0), 1-7.
41. Cho, M. H.; Trottie, J.; Gagnon, C.; Hovington, P.; Clément, D.; Vijh, A.; Kim, C. S.; Guerfi, A.; Black, R.; Nazar, L.; Zaghib, K. *J. Power Sources*, **2014**, 268, 565-574
42. Meini, S.; Piana, M.; Tsiouvaras, N.; Garsuch, A.; Gasteiger, H. A. *Electrochem. Solid-State Lett.* **2012,** 15, (4), A45-A48.
43. Read, J. *J. Electrochem. Soc.* **2006,** 153, (1), A96-A100.
44. Freunberger, S. A.; Chen, Y.; Drewett, N. E.; Hardwick, L. J.; Bardé, F.; Bruce, P. G. *Angew. Chem. Int. Edn.* **2011,** 50, (37), 8609-8613.
45. Laoire, C.; Mukerjee, S.; Plichta, E. J.; Hendrickson, M. A.; Abraham, K. *J. Electrochem. Soc.* **2011,** 158, (3), A302-A308.
46. Xu, D.; Wang, Z.-l.; Xu, J.-j.; Zhang, L.-l.; Wang, L.-m.; Zhang, X.-b. *Chem. Commun.* **2012,** 48, (95), 11674-11676.
47. Walker, W.; Giordani, V.; Uddin, J.; Bryantsev, V. S.; Chase, G. V.; Addison, D. *J. Am. Chem. Soc.* **2013**. 135, 6, 2076–2079
48. Kwabi, D. G.; Batcho, T. P.; Amanchukwu, C. V.; Ortiz-Vitoriano, N.; Hammond, P.; Thompson, C. V.; Shao-Horn, Y. *J. Phys. Chem. Lett.* **2014**, 2850-2856.
49. Chen, S.; Zhu, J.; Han, Q.; Zheng, Z.; Yang, Y.; Wang, X. *Cryst. Growth Des.* **2009,** 9, (10), 4356-4361.
50. Zeng, J.; Nair, J. R.; Francia, C.; Bodoardo, S.; Penazzi, N. *Int. J. Electrochem. Sci* **2013,** 8, 3912-3927.
51. Trahey, L.; Karan, N. K.; Chan, M. K.; Lu, J.; Ren, Y.; Greeley, J.; Balasubramanian, M.; Burrell, A. K.; Curtiss, L. A.; Thackeray, M. M. *Adv. Energy Mater.* **2013,** 3, (1), 75-84.
52. Cui, Y.; Wen, Z.; Liu, Y. *Energy Environ. Sci.* **2011,** 4, (11), 4727-4734.
53. Lee, H.; Kim, Y.-J.; Lee, D. J.; Song, J.; Lee, Y. M.; Kim, H.-T.; Park, J.-K. *J. Mater. Chem. A* **2014**, 2, 11891-11898
54. Thotiyl, M. M. O.; Freunberger, S. A.; Peng, Z.; Chen, Y.; Liu, Z.; Bruce, P. G. *Nature Mater.* **2013,** 12, 1050–1056
55. Benbow, E. M.; Kelly, S. P.; Zhao, L.; Reutenauer, J. W.; Suib, S. L. *J. Phys. Chem. C* **2011,** 115, (44), 22009-22017.
56. Adams, B. D.; Radtke, C.; Black, R.; Trudeau, M. L.; Zaghib, K.; Nazar, L. F. *Energy Environ. Sci.* **2013,** 6, (6), 1772-1778.
57. Park, J.-B.; Hassoun, J.; Jung, H.-G.; Kim, H.-S.; Yoon, C. S.; Oh, I.; Scrosati, B.; Sun, Y.-K. *Nano Lett.* **2013**, 13, 6, 2971–2975
58. Lu, Y.-C.; Kwabi, D. G.; Yao, K. P. C.; Harding, J. R.; Zhou, J.; Zuin, L.; Shao-Horn, Y. *Energy Environ. Sci.* **2011,** 4, (8), 2999-3007.
59. Mitchell, R. R.; Gallant, B. M.; Shao-Horn, Y.; Thompson, C. V. *J. Phys. Chem. Lett.* **2013**, 1060-1064.
60. Zhong, L.; Mitchell, R. R.; Liu, Y.; Gallant, B. M.; Thompson, C. V.; Huang, J. Y.; Mao, S. X.; Shao-Horn, Y. *Nano Lett.* **2013**. 13,5, 2209–2214
61. Black, R.; Lee, J.-H.; Adams, B.; Mims, C. A.; Nazar, L. F. *Angew. Chem. Int. Edn.* **2013,** 52, 392 –396
62. Geaney, H.; O'Connell, J.; Holmes, J. D.; O'Dwyer, C. *J. Electrochem. Soc.* **2014,** 161, (14), A1964-A1968.
63. Geaney, H.; Collins, G.; Glynn, C.; Holmes, J. D.; O'Dwyer, C. *ECS Trans.* **2014,** 58, (12), 21-29.
64. Zhang, Y.; Zhang, H.; Li, J.; Wang, M.; Nie, H.; Zhang, F. *J. Power Sources* **2013,** 240, (0), 390-396.
65. Fan, W.; Cui, Z.; Guo, X. *J. Phys. Chem. C* **2013**, 117, 6, 2623–2627
66. Black, R.; Oh, S. H.; Lee, J.-H.; Yim, T.; Adams, B.; Nazar, L. F. *J. Am. Chem. Soc.* **2012,** 134, (6), 2902-2905.
67. Trahan, M. J.; Mukerjee, S.; Plichta, E. J.; Hendrickson, M. A.; Abraham, K. *J. Electrochem. Soc.* **2013,** 160, (2), A259-A267.

68. Broughton, D. B.; Wentworth, R. L. *J. Am. Chem. Soc.* **1947,** 69, (4), 741-744.

TOC image

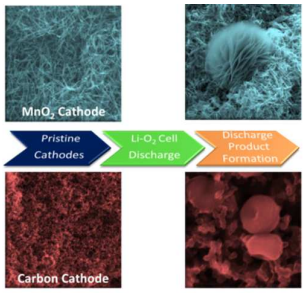

The impact of MnO_2 nanorod catalysts on the nature of discharge products formed in Li-O_2 battery cathodes is examined in anhydrous and water containing electrolytes.